doi:10.1093/brain/awx256

BRAIN
A JOURNAL OF NEUROLOGY

Tau hyperphosphorylation induces oligomeric insulin accumulation and insulin resistance in neurons

Patricia Rodriguez-Rodriguez,[1] Anna Sandebring-Matton,[1] Paula Merino-Serrais,[1] Cristina Parrado-Fernandez,[1] Alberto Rabano,[2,3] Bengt Winblad,[1] Jesús Ávila,[2,4] Isidre Ferrer[2,5] and Angel Cedazo-Minguez[1]

Insulin signalling deficiencies and insulin resistance have been directly linked to the progression of neurodegenerative disorders like Alzheimer's disease. However, to date little is known about the underlying molecular mechanisms or insulin state and distribution in the brain under pathological conditions. Here, we report that insulin is accumulated and retained as oligomers in hyperphosphorylated tau-bearing neurons in Alzheimer's disease and in several of the most prevalent human tauopathies. The intraneuronal accumulation of insulin is directly dependent on tau hyperphosphorylation, and follows the tauopathy progression. Furthermore, cells accumulating insulin show signs of insulin resistance and decreased insulin receptor levels. These results suggest that insulin retention in hyperphosphorylated tau-bearing neurons is a causative factor for the insulin resistance observed in tauopathies, and describe a novel neuropathological concept with important therapeutic implications.

1 Karolinska Institutet, Center for Alzheimer Research, Department of Neurobiology Care Sciences and Society, Division of Neurogeriatrics, Stockholm, Sweden
2 Networking Research Center on Neurodegenerative Diseases (CIBERNED), Instituto de Salud Carlos III, Spain
3 Fundación CIEN, Madrid, Spain
4 Centro de Biología Molecular Severo Ochoa (CSIC-UAM), Madrid, Spain
5 Institut de Neuropatologia, Servei Anatomia Patologica, IDIBELL-Hospital Universitari de Bellvitge, Universitat de Barcelona, Hospitalet de Llobregat, Barcelona, Spain

Correspondence to: Ángel Cedazo-Mínguez
Center for Alzheimer Research, Division of Neurogeriatrics. Department of Neurobiology, Care Sciences and Society, Karolinska Institutet,
NOVUM, 5th floor, SE-14186 Stockholm, Sweden
E-mail: Angel.Cedazo-Minguez@ki.se

Correspondence may also be addressed to: Patricia Rodriguez Rodriguez
E-mail: patricia.rodriguez.rodriguez@ki.se

Keywords: insulin; tau; oligomers; Alzheimer's disease; neurofibrillary tangles

Abbreviations: AGD = argyrophilic grain disease; CBD = corticobasal degeneration; NFT = neurofibrillary tangle; PSP = progressive supranuclear palsy; SIM = structured illumination microscopy

Received April 6, 2017. Revised August 1, 2017. Accepted August 11, 2017.

Introduction

Although the brain was previously considered an insulin-insensitive organ, insulin is now well known to cross the blood–brain barrier through a receptor-mediated saturable transport. The main source of insulin in the brain is peripheral, but some research groups have reported endogenous insulin synthesis in hippocampal neurons and to a less extent in neurons of the cerebral neocortex (Molnár *et al.*, 2014), Purkinje cells of the cerebellar cortex and the granule cell layer of the olfactory bulb (Devaskar *et al.*, 1994). The relevance of insulin in the regulation of glucose uptake and metabolism in the brain has been subject of some controversy, however, very recent reports have shown that knockout (KO) mice for the insulin receptor in astrocytes present decreased glucose transporter-1 (GLUT1) levels, and an overall decrease in glucose consumption in the brain, which suggest that insulin pays a key role in the maintenance of glucose homeostasis in the brain (García-Cáceres *et al.*, 2016). Insulin is also an important neuromodulator that plays an essential role in synaptic plasticity and differentiation (Chiu *et al.*, 2008; Kennedy *et al.*, 2013). Insulin regulates synaptic transmission by promoting the translocation of *N*-methyl-D-aspartate (NMDA) receptors to the cell membrane (Skeberdis *et al.*, 2001) and the internalization of α-amino-3-hydroxy-5-methyl-4-isoxazole-propionic acid (AMPA) receptors (Lin *et al.*, 2000). Moreover, insulin and insulin receptor levels are highly expressed in regions involved in learning and memory, like the hippocampus, where it facilitates long-term potentiation through the activation of the MAPK/ERK pathway (Zhao *et al.*, 2011).

Considering the relevance of insulin for the maintenance of brain homeostasis and function, it is not surprising that alterations in insulin signalling pathways have been associated with Alzheimer's disease. Patients with Alzheimer's disease present reduced CSF-to-plasma insulin ratio (Gil-Bea *et al.*, 2010) and post-mortem analysis of Alzheimer's disease brains has shown downregulated insulin and insulin receptor mRNA levels, together with insulin and insulin receptor substrate 1 (IRS1) signalling impairments (Rivera *et al.*, 2005; Talbot *et al.*, 2012). Furthermore, analysis of neural origin-enriched plasma exosomes has shown an enrichment in pSer312-IRS-1 (associated with ineffective insulin signalling) in Alzheimer's disease patients (Kapogiannis *et al.*, 2015; Mullins *et al.*, 2017). The notion of Alzheimer's disease being a metabolic disorder has gained relevance in the past few years, as increasing evidence suggests that insulin resistance and decreased cerebral glucose utilization are early pathogenic events in the disease. In the past decade, some authors have further suggested that Alzheimer's disease could be a brain-specific type of diabetes (Steen *et al.*, 2005; de la Monte and Wands, 2008). Indeed, fluorodeoxyglucose (FDG)-PET studies have shown that insulin resistance is associated with decreased regional glucose metabolism, especially in the medial temporal lobe, that was associated with worse performance in memory tests (Willette *et al.*, 2015*a*).

Insulin signalling impairment leads to alterations in energy metabolism and increased oxidative and endoplasmic reticulum stress (De La Monte *et al.*, 2012), all common features of neurodegenerative disorders like Alzheimer's disease. Furthermore, deficits in insulin signalling are a contributing factor to tau hyperphosphorylation and neurofibrillary tangle (NFT) formation (Calvo-Ochoa *et al.*, 2014). Insulin regulates tau phosphorylation by modulating the activity of tau kinases, including glycogen synthase kinase 3 beta (GSK3β) through the phosphatidylinositol kinase (PI3K)/protein kinase B (AKT) signalling pathway (Schubert *et al.*, 2004; Avila, 2008; Liu *et al.*, 2008; Bian *et al.*, 2016). Insulin resistance leads to aberrant GSK3β activation (Schubert *et al.*, 2004) and inhibition of AMPK-mediated tau de-phosphorylation (Kim *et al.*, 2015), triggering tau hyperphosphorylation. Moreover, the decrease in glucose metabolism as a consequence of insulin resistance leads to tau *O*-GlcNAcylation downregulation, contributing to tau hyperphosphorylation (Liu *et al.*, 2004, 2009; Yuzwa and Vocadlo, 2014). Insulin-signalling deficiencies have also been shown to predict the pathological deposition of amyloid-β, another key feature in Alzheimer's disease (Willette *et al.*, 2015*b*). Insulin promotes the non-amyloidogenic processing of amyloid precursor protein (APP) by regulating its phosphorylation, thus, defects in insulin signalling can increase pathological amyloid-β accumulation (Pandini *et al.*, 2013). Furthermore, insulin and amyloid-β are both substrates of insulin-degrading enzyme (IDE). Insulin regulates IDE by increasing its protein levels, thus deficits in insulin signalling lead to deficient amyloid-β degradation (Zhao *et al.*, 2004, 2009).

Despite the fact that insulin has been shown to be essential for neuronal function and memory formation and that deficiencies in insulin signalling have been directly linked to some of the major hallmarks of neurodegenerative disorders like Alzheimer's disease, to date, little is known about insulin state and distribution under pathological conditions in the brain. Here, we report that insulin is accumulated and retained as insoluble oligomers in tau-bearing neurons in Alzheimer's disease and several of the most prevalent tauopathies. Intraneuronal insulin accumulation is driven by tau hyperphosphorylation and results in insulin resistance. The implications of these findings to the pathogenesis of tauopathies and their relevance for proposed insulin-based therapies are discussed.

Materials and methods

Human brain samples

Paraffin-embedded brain slices from the cingulate cortex, frontotemporal cortex and hippocampus of non-diabetic patients with Alzheimer's disease, patients with definite Alzheimer's

disease and diabetes mellitus, control patients and control patients with diabetes mellitus were obtained from the CIEN foundation Brain Bank (Spain). Paraffin-embedded hippocampal slices from Alzheimer's disease patients with Braak I–II, Alzheimer's disease Braak III–IV, Alzheimer's disease Braak V–VI, hippocampal slices of patients with argyrophilic grain disease (AGD), patients with progressive supranuclear palsy (PSP) (hippocampus and striate nucleus) and patients with corticobasal degeneration (CBD) (hippocampus and frontal cortex) were provided by the Bellvitge University Hospital (Spain). Fresh frozen human brain specimens of different regions were obtained from the Harvard Brain Tissue Resource Center (MA, USA). The post-mortem intervals, neuropathological and clinical diagnoses, age and gender distribution as well as diagnostic grouping are presented in Table 1.

Mice tissue

Sagittal sections (30 µm) of brain tissue were obtained from 3 month tau-KO (Charles Rivers) and 10-month-old PS19

Table 1 Demographic data of the cases studied

Diagnosis	Age	Gender	PMI (h)	Braak stage	DM	APOE	Analysis	Source
Ctrl_1	81	M	23.33	II	-	-	ELISA, WB	Harvard Brain Tissue Resource Center (USA)
Ctrl_2	72	M	27.67	I	–	–	ELISA, WB	Harvard Brain Tissue Resource Center (USA)
Ctrl_3	82	F	24.42	II	–	–	ELISA, WB	Harvard Brain Tissue Resource Center (USA)
Ctrl_4	73	F	24.88	I	–	–	ELISA, WB	Harvard Brain Tissue Resource Center (USA)
Ctrl_5	71	F	22.00	I	–	–	ELISA, WB	Harvard Brain Tissue Resource Center (USA)
Ctrl_6	82	–	9	I	–	E3/E3	IP/WB	Karolinska Institutet Brain Bank (Sweden)
Ctrl_7	80	F	7	I	–	E3/E3	IP/WB	Karolinska Institutet Brain Bank (Sweden)
Ctrl_8	83	F	9	I	–	E3/E3	IP/WB	Karolinska Institutet Brain Bank (Sweden)
Ctrl_9	75	M	5	I	ND	–	IF, IHC	CIEN foundation (Spain)
Ctrl_10	78	F	3	III	ND	–	IF	CIEN foundation (Spain)
Ctrl_11	88	M	3	II	ND	–	IF	CIEN foundation (Spain)
Ctrl_12	74	F	7	–	ND	–	IF, IHC	CIEN foundation (Spain)
Ctrl_13	–	–	2	–	DM	–	IF	CIEN foundation (Spain)
Ctrl_14	–	–	2	–	DM	–	IF	CIEN foundation (Spain)
AD_1	76	F	8	VI	–	–	ELISA, WB	Harvard Brain Tissue Resource Center (USA)
AD_2	68	M	8.62	VI	–	–	ELISA, WB	Harvard Brain Tissue Resource Center (USA)
AD_3	85	F	25.26	VI	–	–	ELISA, WB	Harvard Brain Tissue Resource Center (USA)
AD_4	82	M	12.88	V	–	–	ELISA, WB	Harvard Brain Tissue Resource Center (USA)
AD_5	71	F	27	V	–	–	ELISA, WB	Harvard Brain Tissue Resource Center (USA)
AD_6	84	F	25.50	V	–	–	ELISA, WB	Harvard Brain Tissue Resource Center (USA)
AD_7	72	F	8	V	–	–	IP/WB	Karolinska Institutet Brain Bank (Sweden)
AD_8	70	F	12	V	–	–	IP/WB	Karolinska Institutet Brain Bank (Sweden)
AD_9	76	–	4	VI	–	E3/E4	IP/WB	Karolinska Institutet Brain Bank (Sweden)
AD_10	74	F	4	V	DM	E3/E4	IF	CIEN foundation (Spain)
AD_11	82	F	4.3	V	DM	E3/E4	IF	CIEN foundation (Spain)
AD_12	80	M	–	V	DM	E3/E4	IF	CIEN foundation (Spain)
AD_13	86	F	3	V	ND	E3/E3	IF, IHC	CIEN foundation (Spain)
AD_14	84	F	3	V	ND	E3/E3	IF, IHC	CIEN foundation (Spain)
AD_15	84	F	6	VI	ND	E3/E3	IF	CIEN foundation (Spain)
AD_16	52	F	11	I–II	–	–	IF	Bellvitge University Hospital (Spain)
AD_17	77	F	17.40	I–II	–	–	IF	Bellvitge University Hospital (Spain)
AD_18	69	F	11.40	I–II	–	–	IF	Bellvitge University Hospital (Spain)
AD_19	72	F	16.10	III–IV	–	–	IF	Bellvitge University Hospital (Spain)
AD_20	89	M	3.20	III–IV	–	–	IF	Bellvitge University Hospital (Spain)
AD_21	69	F	8	III–IV	–	–	IF	Bellvitge University Hospital (Spain)
AD_22	96	F	17.35	V–VI	–	–	IF	Bellvitge University Hospital (Spain)
AD_23	73	F	17.45	V–VI	-	-	IF	Bellvitge University Hospital (Spain)
AD_24	75	M	21.14	V–VI	-	-	IF	Bellvitge University Hospital (Spain)
PSP_1	56	M	11.25	Advanced	-	-	IF	Bellvitge University Hospital (Spain)
PSP_2	65	M	8.45	Advanced	-	-	IF	Bellvitge University Hospital (Spain)
CBD_1	83	M	13.35	Advanced	-	-	IF	Bellvitge University Hospital (Spain)
AGD_1	79	M	24.30	Advanced	-	-	IF	Bellvitge University Hospital (Spain)
AGD_2	63	M	10.20	Advanced	-	-	IF	Bellvitge University Hospital (Spain)
AGD_3	82	F	4	Advanced	-	-	IF	Bellvitge University Hospital (Spain)

I-VI = Braak stages; AD = Alzheimer disease; Ctrl = Control; DM = diabetes mellitus; F = females; IF = immunofluorescence; IHC = immunohistochemistry; IP = immunoprecipitation; M = males; ND = non-diabetic; PMI = post-mortem interval; WB = western blot; – = no information available.

mice encoding the human P301S mutation (The Jackson Laboratory, 008169). P301S mice were back-crossed for eight generations with C57BL6/J mice. Wild-type (WT) animals (C57BL6/J) of respective similar ages were used as controls. The P301S mouse model carries a mutant (P301S) human *MAPT* gene encoding T34-tau isoform (1N4R) driven by the mouse prion-protein promoter (*Prnp*) on a B6C3H/ F1 genetic background (Yoshiyama *et al.*, 2007). Tau-KO was generated by replacing exon 1 of the mouse TAU gene with a neomycin resistance cassette34 (Dawson *et al.*, 2001). All mice were housed at the Centro de Biologıa Molecular 'Severo Ochoa' animal facility. Mice were housed four per cage with food and water available *ad libitum* and maintained in a temperature-controlled environment on a 12/12 h light-dark cycle with light onset at 07:00 h. Animal housing and maintenance protocols followed the guidelines of Council of Europe Convention ETS123, recently revised as indicated in the Directive 86/609/EEC. Animal experiments were performed under protocols (P15/P16/ P18/P22) approved by the Centro de Biologıa Molecular Severo Ochoa Institutional Animal Care and Utilization Committee (Comite de Etica de Experimentación Animal del CBM, CEEA-CBM, Madrid, Spain).

Cell lines

SH-SY5Y human neuroblastoma cell line was obtained from the American Type Culture Collection (ATCC). Stable full-length tau (Tau 441) overexpressing SH-SY5Y (SH-SY5Y-Tau) cells were created as described by Monroy-Ramírez *et al.* (2013).

Cells were grown in a 1:1 Dulbecco's modified Eagle medium: Nutrient Mixture F-12 (DMEM/F-12) (Thermo-Fisher) supplemented with 10% foetal bovine serum (Thermo-Fisher) and incubated at 37°C in a humidified 5% CO_2-containing atmosphere. Cells were seeded (150 000 cells/cm^2) 24 h before the experiments.

Primary cultures

Cortical neurons in primary culture were prepared from foetal (embryonic Day 18) Wistar rats (Jackson). Cells were seeded (25 000 cells/cm^2) in Neurobasal® media (Thermo Fisher), supplemented with 2% B-27® (Thermo Fisher), 2 mM GlutaMAX™ (Thermo Fisher), 100 units/ml penicillin and 100 µg/ml streptomycin (PEST, Thermo Fisher), and incubated at 37°C in a humidified 5% CO_2-containing atmosphere. All experiments were performed after 10 days in culture. All the experiments involving primary cultures were approved by Karolinska Institute's regional ethical committee.

Cell treatments

For okadaic acid treatments, media was removed and replaced with complete media (Neurobasal®, 2% B-27®, 2 mM GlutaMAX™) with 250 nM of okadaic acid (O9381, Sigma-Aldrich) prepared in DMSO (O9381, Sigma-Aldrich). Media with the same final concentration of DMSO was used as a control. The cells were then incubated for 1 h at 37°C in a humidified 5% CO_2-containing atmosphere.

Cell transfections

Short interfering RNA (siRNA) transfections in rat cortical neurons in primary culture were performed using the reagent DharmaFECT™ (Thermo Fisher) following the manufacturer's instructions. Tau siRNA (50 nM) (L-089500-02-0005; Darmacon) and DharmaFECT™were incubated separately for 5 min in Neurobasal® complete media. They were then mixed and incubated for 20 min. The Darmafect-siRNA mix was then added to the cells. Transfection controls were performed with a non-targeting siRNA (D-001810-10-05 Darmacon). Experiments were performed after 72 h of transfection when tau silencing was up to 50%.

SH-SY5Y cells were transfected with 1 µg/ml plasmid vectors using Lipofectamine® 3000 reagent (Thermo Fisher), following the manufacturer's instructions. Plasmids encoding GFP-tagged human tau (pRK5-EGFP-Tau, Addgene plasmid #46904), GFP-tagged pseudo-phosphorylated tau (pRK5-EGFP-Tau E14, Addgene plasmid #46907) and GFP-tagged phospho-null tau (pRK5-EGFP-Tau AP, Addgene plasmid #46905) were a gift from Karen Ashe. pRK5-EGFP-Tau plasmid contains 4R0N human tau sequences, pRK5-EGFP-Tau E14 and pRK5-EGFP-Tau AP contain human tau sequence with mutations in serine and proline amino acid residues (T111, T153, T175, T181, S199, S202, T205, T212, T217, T231, S235, S396, S404 and S422) to glutamate (E14) or alanine (AP) (Hoover *et al.*, 2010). Transfections with pcDNA 3 were used as control. Cells were used for the experiments 48 h after transfection.

Immunofluorescence

Cells were seeded in poly-D-lysine-coated round glass coverslips. After the treatments, they were fixed in 4% PFA for 10 min. Fixed cells were then blocked for 30 min in 1% bovine serum albumin (BSA), 0.1% Triton™ X-100, phosphate-buffered saline (PBS, Thermo Fisher) and incubated with the primary antibody overnight at 4°C. The antibodies used were Insulin (1:300; ab7842, Sigma-Aldrich) and AT180 (1:500; NB100-82249, Novus Biologicals). The day after, the cells were washed with PBS and incubated with the secondary antibody in PBS for 1 h at room temperature. The secondary antibodies used were Alexa Fluor® 488 goat anti-guinea pig (1:1000, Invitrogen corporation) and Alexa Fluor® 633 goat anti-rabbit (1:1000, Invitrogen corporation). DAPI was used as nuclear staining. Cells were then washed and mounted with ProLong® Gold Antifade Reagent (Thermo Fisher).

Paraffin-embedded brain slices (14 µm) were deparaffinized by xylene (twice, 10 min each) followed by 90% ethanol (twice, 10 min each), 70% ethanol (10 min) and finally distilled H_2O (10 min) incubations. Antigen retrieval was later performed using the DIVA NxGen decloaker and DIVA reagent (DV2004MX, Biocare Medical) for 30 min at 110°C in a Decloaking Chamber™ NxGen (DC2012, Biocare Medical). Brain slices were then permeabilized in PBS, 0.1% Triton™ X-100 for 30 min. They were then blocked with PBS, 0.05% Triton™ X-100, 10% goat serum for 30 min and incubated with the primary antibody in PBS, 0.05% Triton™ X-100, 10% goat serum overnight at 4°C. The antibodies used were Insulin (1:300; ab7842, Sigma-Aldrich and 1:100; Ab909, Bio-YEDA), AT180 (1:500; NB100-82249, Novus Biologicals), GFAP (1:300; 556330, BD Pharmigen), Tau-1 (1:300;

MAB3420, Sigma-Aldrich) and AT100 (1:300; MN1060, Thermo Fisher). The day after, slices were washed in PBS and incubated with secondary antibodies in PBS for 1 h and 30 min at room temperature. The secondary antibodies used were Alexa Fluor® 488 goat anti-guinea pig (1:1000, Invitrogen), Alexa Fluor® 633 goat anti-guinea pig (1:1000, Invitrogen corporation), Alexa Fluor® 546 goat anti-mouse (1:1000, Invitrogen corporation), Alexa Fluor® 633 goat anti-rabbit (1:1000, Invitrogen corporation) and Alexa Fluor® 405 goat anti-mouse (1:1000, Invitrogen). DAPI was used as nuclear staining. After incubations with secondary antibodies we stained with Milli-Mark™ FluoroPan Neuronal Marker-Alexa488 conjugate (MAB2300X, Millipore). Afterwards, the slices were washed in PBS. To eliminate lipofuscin autofluorescence, eliminator reagent (2160, Millipore) was used following the manufacturer's instructions. Finally, they were mounted with ProLong® Gold Antifade Reagent (Thermo Fisher).

Avidin-biotin complex staining

Paraffin-embedded slices (4 µm) were deparaffinized by xylene (twice, 10 min each) followed by 90% ethanol (twice, 10 min each), 70% ethanol (10 min) and finally distilled H_2O (10 min) incubations. Afterwards, antigen retrieval was performed using the DIVA NxGen decloaker and DIVA reagent (DV2004MX, Biocare Medical) for 30 min at 110°C. Brain slices were then permeabilized in PBS, 0.1% Triton™ X-100 for 30 min. Endogenous peroxidase activity was blocked by 5 min incubation with a peroxidase-blocking reagent (K4010, Dako). They were then blocked with PBS, 0.05% Triton™ X-100, 10% goat serum for 30 min and incubated with insulin primary antibody (1:300; ab7842, abcam) in PBS, 0.05% Triton™ X-100, 10% goat serum overnight at 4°C. The day after slices were washed in PBS and incubated with the biotinylated secondary antibody (1:1000; BA-7000, Vector Laboratories) for 1 h and 30 min at room temperature. The slices were then washed with PBS and incubated for 30 min with avidin-biotin complex (ABC) reagent (PK-6100, Vector Laboratories). The samples were then incubated in liquid DAB + chromogen solution for detection (K4010, Dako). The reaction was stopped by H_2O_2 washing. Afterwards the tissue was dehydrated by sequential incubations with 70% ethanol (twice, 3 min), 90% ethanol (10 min) and xylene (twice, 10 min). Finally, they were mounted with DEPEX.

Imaging

Confocal imaging was performed with a Zeiss LSM 510 META confocal laser scanning system. The fluorescence was recorded sequentially in separate channels with Plan-Apochromate 20× (NA, 0.8), 40× (NA, 1.2) oil and 100× (NA, 1.45) oil objectives. Image processing was performed with the included ZEN software. Cell quantifications were performed with Neurolucida. Fluorescence intensity was measured with the ImageJ 1.383 software (NIH, MA, USA).

Super-resolution structured illumination microscopy (SIM) was performed at the Super-Resolution Microscopy Science for Life Laboratory (Stockholm, Sweden) on a Carl Zeiss Elyra PS.1 microscope. This method consists of generating a grid by illuminating the sample with specially structured excitation light. Afterwards it is processed to generate a reconstruction with improved resolution (Gustafsson, 2000). It can resolve an eight times smaller volume than conventional confocal microscopy without using special fluorophores, and has been shown to be the most suitable super-resolution technique for imaging densely packed structures, as is the case with NFTs (Schermelleh *et al.*, 2010; Wegel *et al.*, 2016). The objective used was an oil Plan-Apochromate 63× (NA, 1.40). Emission was collected sequentially through appropriate dichroic mirrors and band pass filters set at 570–650 nm (561 nm excitation) and 495–575 nm (488 nm excitation). SIM processing was done with the included ZEN software with selection of automatic settings for evaluation of the raw data (i.e. theoretical PSF, selection of noise filter setting, frequency weighting, baseline settings etc.) (Komis *et al.*, 2015). The optimal grid size was automatically assigned to each wavelength by the Zeiss Zen software, and the grid was rotated five times at five phases for each image. After evaluation, the SIM images were checked for possible artefacts (e.g. honey comb patterns of intensity in the image) so appropriate selections of evaluation settings were applied. Calibration on 40 nm beads generated a lateral precision of $\sim 97 \pm 4$ nm at 488 nm excitation.

Optical imaging was performed on a Nikon Eclipse E800M optical microscope with a Plan-Apochromate 20× (NA, 0.75) objective.

Western blot

After the treatments, cells were lysed in 1% Triton™ X-100, 150 mM NaCl, 1 mM EDTA, 1 mM EGTA, 50 mM Tris; pH 7.5, supplemented with phosphatase and protease inhibitors (Sigma-Aldrich). The cell extracts were then subjected to sodium dodecyl sulphate (SDS) polyacrylamide gel electrophoresis (MiniProtean, Bio-Rad) and transferred to a nitrocellulose membrane (GE healthcare). Membranes were blocked in 5% non-fat milk for 1 h at room temperature and blotted with the primary antibodies overnight at 4°C. Antibodies used were Insulin (1:2000; NBP1-45662, Novus Biologicals), Total Tau (1:1000; A0024, Dako), AT180 (1:2000; NB100-80249, Novus Biologicals), Insulin degrading enzyme (IDE) (1: 1000; sc-27265, Santa Cruz Biotechnology), Insulin receptor beta (total IR) (1:1000; Cell Signalling) and phospho Akt (P-Akt) (1:1000; 9271S, Cell Signalling). Actin (1:5000; A2066, Sigma-Aldrich) or GAPDH (1:2000; ADI-CSA-335, Enzo) were used as loading controls. The day after, they were incubated with horseradish peroxidase-conjugated goat anti-mouse (1:5000; NA941V, GE healthcare), goat anti-rabbit (1:5000; NA934V, GE healthcare) or donkey anti-goat (1:5000; PI9500, Vector Laboratories) antibodies for 1 h at room temperature. Signal detection was performed with an enhanced chemiluminescence kit (ECL detection system, Amersham Biosciences). The quantification of the bands was performed with the ImageJ 1.383 software and calculated from the optical density multiplied by the area for each band. The values were then normalized with their corresponding loading control (actin or GAPDH).

Immunoprecipitation

Insulin (1:200; NBP1-45662, Novus Biologicals) or A11 pan-oligomers (1:100; AHB0052, Invitrogen) antibodies were incubated with 20 µl of Dynabeads® protein A (Thermo Fisher) in

an orbital shaker (overnight, 4°C). Afterwards the antibody-beads conjugate was washed with PBS and incubated with the protein lysates (0.25 µg/µl, obtained as detailed in the western blot section) overnight at 4°C in an orbital shaker. The following day, an aliquot of the supernatant was retired for using as loading control (input). The remaining supernatant was then removed and the beads-antibody-protein pellet was washed three times with PBS. Finally, the proteins were eluted from the antibody by incubation in loading buffer (10 min at 70°C), subjected to native PAGE (for insulin immunoprecipitation) or SDS (for A11 immunoprecipitation) polyacrylamide gel electrophoresis, transferred to a nitrocellulose membrane and blotted against A11 (insulin immunoprecipitation) or insulin (A11 immunoprecipitation). To determine the specificity of the A11 antibody for oligomeric forms of insulin, three controls were used in the immunoprecipitation process: PBS, 1 µg/µl human recombinant insulin (91077C, Sigma-Aldrich) and the same concentration of human recombinant insulin that had been previously incubated for aggregation (24 h, 37°C in an orbital shaker). The presence of insulin aggregates in this sample was confirmed by thioflavin fluorescence assays (data not shown).

Preparation of human samples for ELISA analysis

Preparation was done from 100 mg of frozen human hippocampus of control ($n = 4$) and Alzheimer's disease ($n = 5$) cases (Table 1) homogenized in 600 µl PBS (pH 7.4) using a pestle motor homogenizer (Sigma-Aldrich). Homogenization was performed at + 4°C in presence of protease and phosphatase inhibitor cocktails (Sigma-Aldrich) until completely dissolved (~1 min at full speed). The whole volume of brain homogenate was centrifuged at 125 000*g* for 20 min. The supernatant (PBS fraction) was collected and the pellet dissolved in 150 µl 1% SDS in PBS and centrifuged at 125 000*g* for 20 min at room temperature. This step was repeated until six SDS soluble fractions were obtained. The SDS supernatants were pooled for subsequent analysis (SDS fraction). The remaining pellet of insoluble material was immediately dissolved in 80% formic acid (FA), vortexed for 30 s followed by 20 min sonication in a 20°C water bath. After 25 000*g* centrifugation for 10 min, the supernatant was collected (formic acid fraction). All samples were stored at –20°C until further analysis. Immediately before the ELISA measurements, formic acid soluble fractions were neutralized in 2 M Tris-HCl, pH 14.0 and mixed with 10 × radio-immunoprecipitation assay (RIPA) buffer (750 mM NaCl/5.0% NP-40/2.5% sodium deoxycholate/0.5% SDS/250 mM Tris–HCl, pH 8.0) to avoid peptide aggregation.

Enzyme linked immunosorbent assay

Insulin concentrations in PBS, SDS and formic acid fractions were measured in duplicates by human Insulin ELISA kit (Merck Millipore) following the manufacturer's instructions. A volume of 100 µl of undiluted PBS and SDS samples and a 10-fold dilution of the formic acid samples were loaded to the ELISA plate and incubated at room temperature for 90 min on orbital shake (400 rpm). After a series of washing with wash buffer supplied in the kit, human insulin detection antibody was added to each well and incubated for 1 h at room temperature. After washing, the wells were incubated with enzyme solution for 30 min and the amount of insulin was subsequently quantified by incubating with 50 µM Amplex® UltraRed reagent (Invitrogen) for 30 min, followed by detection of the fluorescent signal using a 544 nm excitation filter and 590 nm emission filter in a microplate reader (TECAN). The data were normalized to protein content in each fraction. Total insulin without normalization is illustrated in Supplementary Fig. 1F.

Protein determination

Protein contents were determined using Pierce BCA kit (Thermo Scientific) according to the manufacturer's instructions.

Relative quantification in real time

Total RNA was isolated using the RNeasy® mini kit (Qiagen) including DNAse treatment (RNase-Free DNase Set, Qiagen). RNA samples were run on agarose gels to confirm no genomic DNA contamination and the purity was assessed by RNA 260/280 ratio. Total RNA (300 ng) was then reverse transcribed using High Capacity cDNA Reverse Transcription kit (Applied Biosystems). To perform real time RT-qPCR assays, we used the relative standard method supplied by Applied Biosystem (Applied Biosystems, 2004). Serial dilutions of a reverse transcription product (cDNA) from rat brain were carried out to obtain standards curves containing 100, 50, 5, 0.5, 0.05 ng/µl, and run by duplicate in the same PCR plate as the experimental samples. PCR reactions were performed to quantify both target gene (Ins2 and InsR) and endogenous gene (*Gapdh*) sequences in three independent experiments. Relative quantities of *Slc2a4* (GLUT4), *Ins2*, *Insr* mRNA and *Gapdh* mRNA were determined by comparing the threshold cycle (Ct) of each sample with that of a standard curve run on the same PCR plate. Thermocycling and fluorescence detection was performed according to the TaqMan® Gene Expression Assays Protocol using an ABI PRISM® 7000 Sequence Detection System with a total volume of 20 µl in each well containing 10 µl of PCR Master Mix (Applied Biosystems), 2 µl of cDNA (corresponding to 15 ng of total RNA), 1 µl of each TaqMan® Gene Expression Assays primer (Applied Biosystems), and 7 µl molecular grade RNase-free water (Dharmacon GE Lifesciences, B-003000-WB-100). Relative quantities of target genes were adjusted to relative quantities of *Gapdh* and normalized to controls conditions (set at 100%). Values are reported as the mean ± SEM (standard error of the mean) of triplicate experiments. $***P < 0.001$; $**P < 0.01$; $*P < 0.05$ indicate values that significantly differ from controls.

Flow cytometry

For FITC-Insulin uptake experiments neurons in primary culture were incubated for 1 h in Neurobasal® media (Thermo Fisher), supplemented with 2% B-27® minus insulin (Thermo Fisher), 2 mM GlutaMAX™ (Thermo Fisher) and 400 nM FITC-labelled insulin (I3661, Sigma-Aldrich), either in the presence or absence of okadaic acid (250 nM), at 37°C in a humidified 5% CO_2-containing atmosphere. Neurons where then detached with 5 mM EDTA. After centrifugation (500*g*, 5 min) they were resuspended in PBS and insulin fluorescence

intensity (an average of 20 000 cells per condition in five different experiments) was measured on a FACScalibur™ flow cytometer (15 mW argon ion laser tuned at 488 nm; CellQuest software, Becton Dickinson Biosciences).

Statistical analysis

Measurements were carried out in duplicate or triplicate. The results are expressed as mean ± SEM values for three different cell culture/clinical sample preparations. The statistical analysis of the results was performed by one-way analysis of variance (ANOVA), followed by the least significant difference multiple range test. In all cases, $P < 0.05$ was considered to be significant ($*P < 0.05$, $**P < 0.01$).

Results

Insulin is accumulated in hyperphosphorylated tau-bearing neurons in Alzheimer's disease

Regarding the close relationship between insulin resistance and Alzheimer's disease, we first aimed to determine if insulin distribution was affected in Alzheimer's disease brains by performing immunohistochemical staining for insulin in different areas (cingulate cortex, temporal cortex and hippocampus) of control (Cases Ctr_10–12) and Alzheimer's disease (Cases AD_13–15) brains. These areas were selected according to the progression of tau pathology in Alzheimer's disease, which initiates in the entorhinal cortex, continues in the hippocampus and reaches neocortical regions in the most advanced stages of the disease (Braak and Braak, 1996). As seen in Fig. 1A, insulin immunoreactivity was widely distributed and showed stronger staining in Alzheimer's disease brains compared to controls, particularly in the hippocampus (CA1–CA3). In neocortical areas, similar results were found in the temporal cortex (layer III), being less evident in the cingulate cortex (Supplementary Fig. 1A). Double immunofluorescence analysis of the CA1 hippocampal layer for insulin, glial fibrillary acidic protein (GFAP) and FluoroPan neuronal marker revealed that Alzheimer's disease brains (Cases AD_14–15 and 22) had higher insulin staining in neurons compared to controls. In contrast, control brains (Ctr_9–11) showed stronger insulin immunoreactivity in astrocytes compared to neurons and no differences were found in insulin staining in astrocytes in Alzheimer's disease compared to controls (Fig. 1B). As shown in Supplementary Fig. 1C, insulin was not present in extracellular tau deposits or thioflavin S-positive plaques (data not shown).

To further explore if brain insulin accumulation follows tau pathology progression, we performed immunofluorescence studies in hippocampal slices from patients in early to late stages of the disease (Braak I–VI). As shown in Fig. 1C and Supplementary Fig. 1D, insulin immunofluorescence intensity was significantly increased in the CA1 layer of the hippocampus in initial (Braak I–II) through advanced stages of Alzheimer's disease (Braak V–VI) (Ctr_10–14 and Cases AD_16–24). It is noteworthy that we performed immunohistochemical studies using a different insulin antibody (Ab909) with comparable results (Supplementary Fig. 1B).

Given that type 2 diabetes mellitus (T2DM) and hyperinsulinemia are known risk factors for Alzheimer's disease (Luchsinger *et al.*, 2004; Xu *et al.*, 2004), we explored the possible relationship between T2DM and brain insulin accumulation in a subset of samples from controls (Ctr_9–14) and Alzheimer's disease (AD_10–15) individuals with and without T2DM. To do so, we established criteria for basal insulin fluorescence intensity (arrows in Supplementary Fig. 1E), the cells where insulin staining was found to be stronger were considered as cells with increased insulin levels (asterisks in Supplementary Fig. 1E). The total number of cells was counted per image field in a total of three images from the CA1 layer of the hippocampus per patient, and each cell (70 cells on average) classified depending on its insulin status. As shown in Fig. 1D, the percentage of cells with accumulated insulin was significantly increased in Alzheimer's disease patients regardless of T2DM status. Furthermore, the number of neurons with accumulated insulin was lower in control brains regardless of their T2DM.

We next investigated whether insulin accumulation occurs in the same neurons bearing tau hyperphosphorylation. To detect tau pathology, we used AT180, an antibody that recognizes hyperphosphorylated tau at T231. Figure 1E shows insulin and AT180 immunoreactivities in the CA1 hippocampal layer of control and Braak V–VI. In Alzheimer's disease samples, insulin levels were higher in AT180 positive neurons, especially in those with NFT-like staining (Fig. 1E). As seen in Fig. 1F, quantification of immunoreactivities in layer III of the cingulate and temporal cortices as well as hippocampal CA1 from Alzheimer's disease (AD_10–15) and controls (Ctr_9–12) revealed that insulin accumulation was not present in all neurons with NFT formations. Interestingly, the majority of neurons with high insulin levels (~80–90%) also showed NFTs. Consistent with the findings showed in Fig. 1A and Supplementary Fig. 1A, hippocampal neurons displayed higher insulin accumulation (~60% of total neurons) compared to neocortical areas (~30%) (Fig. 1F). Quantification of insulin status was performed using the criteria shown in Supplementary Fig. 1E. Considering that AT180 has been shown to be highly conserved in MAP2 (Xie and Miyasaka, 2016), we performed additional staining with another anti-hyperphosphorylated tau antibody (AT100) and with total tau (Tau-1) in the hippocampus of control and Alzheimer's disease patients. In all the cases studied, AT180 co-localizes with AT100 immunoreactivity, discarding the exclusion of phospho-tau positive neurons, and possible artefacts due to the interaction of AT180 with MAP2 (Supplementary Fig. 2A). Furthermore, CA1-CA3 hippocampal neurons with NFT also showed increased Tau-1

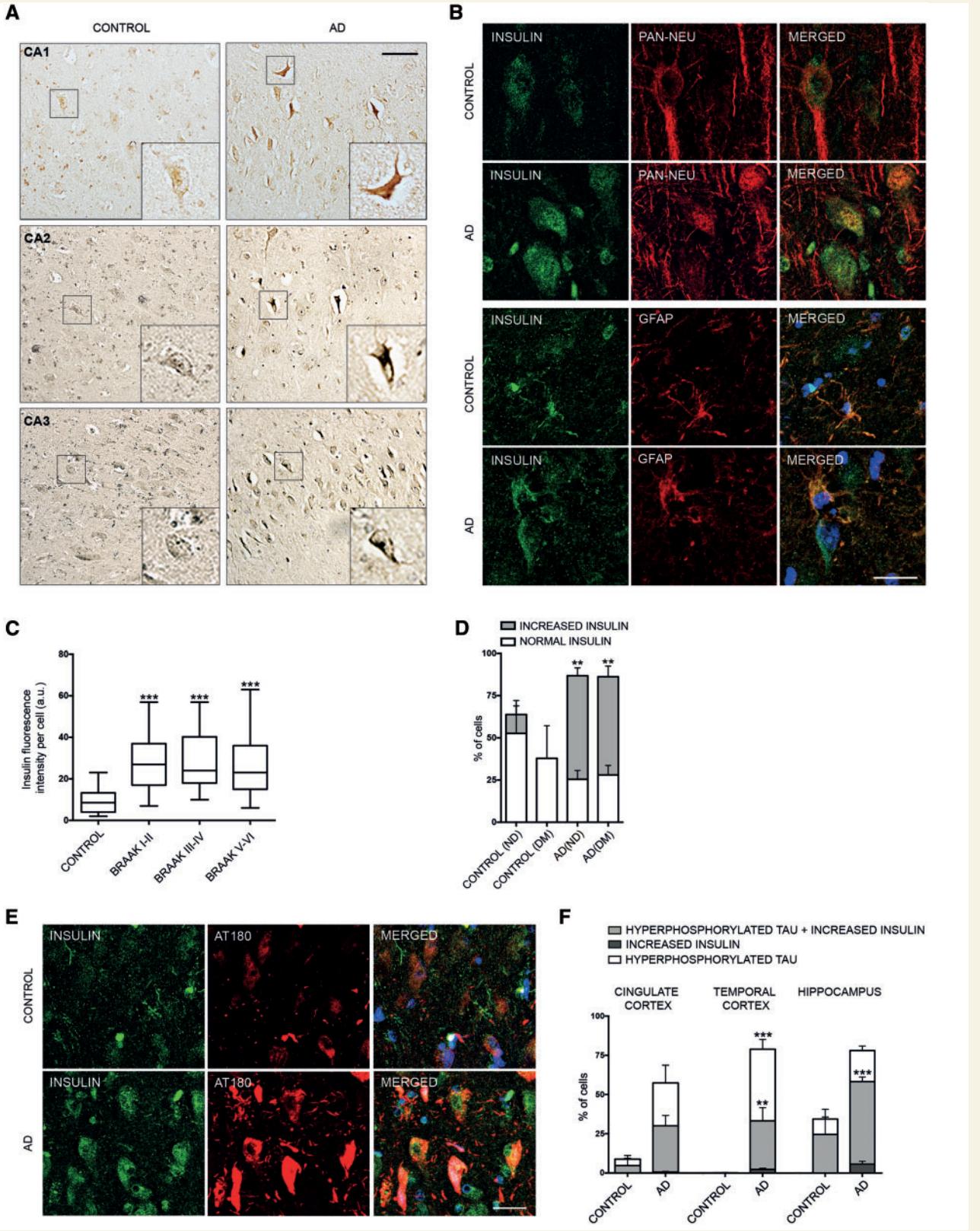

Figure 1 Insulin levels are increased in hyperphosphorylated tau-bearing hippocampal and cortical neurons in Alzheimer's disease. (**A**) ABC immunohistochemistry for insulin in human brain sections of the CA1, CA2 and CA3 layers of the hippocampus show increased insulin staining in Alzheimer's disease samples compared to controls. Scale bar = 100 μm. (**B**) Confocal microscopy images of insulin (green), Pan-neuronal marker (red) and GFAP (red) in CA1 of control and Alzheimer's disease patients. In neurons, insulin is increased in Alzheimer's disease and barely detectable in controls. In astrocytes, insulin immunoreactivity was detected both in controls and Alzheimer's disease. DAPI (blue) was used as nuclear marker. Scale bar = 25 μm. (**C**) Insulin fluorescence intensity quantification from confocal images in

(continued)

immunoreactivity in Alzheimer's disease, suggesting tau pathological accumulation (Supplementary Fig. 2B).

Insulin accumulates as oligomers in the brain

We and others have previously reported decreased insulin levels in the CSF of Alzheimer's disease individuals (Gil-Bea *et al.*, 2010; Lee *et al.*, 2013), which seems in apparent contrast to the results presented above. To further clarify this issue, we measured insulin levels in brain fractions of different solubility. Based on a modified protocol for separating different forms of amyloid-β from human brain (Sandebring *et al.*, 2013), we extracted PBS (monomers and soluble oligomers), SDS (water insoluble oligomers and protofibrils) and formic acid (large, fibrillar structures and insoluble oligomers) fractions from hippocampal brain samples of controls (Ctrl_1–5) and Alzheimer's disease (AD_1–6) individuals and quantified insulin levels by ELISA. Data were normalized to the protein content of each fraction. Two cases (one control and one Alzheimer's disease) were excluded as outliers as they were not within the interquartile range by >1.5 of interquartile ranges (Williamson *et al.*, 1989).

As shown in Fig. 2A, the total pool of insulin in control brains was mainly distributed in the PBS (51%) and SDS (32%) fractions, while formic acid-enriched insulin accounted for ~17%. Interestingly, a significantly higher insulin accumulation was detected in formic acid fractions from Alzheimer's disease cases compared to controls (Fig. 2B). No differences between groups were found in SDS-soluble fractions. In the PBS fractions, we observed a slight increase in the Alzheimer's disease group that was not significant when normalized by total protein levels (Supplementary Fig. 1F). It is worth noting that differences in total protein content between Alzheimer's disease and control brains due to neuronal cell death, massive gliosis and increased protein aggregation make proper data normalization difficult. Figure 2C shows the levels of the neuronal marker NeuN, the glial marker GFAP and actin in the PBS and SDS fractions. As expected, there was a significant reduction in the number of neurons and extensive gliosis in Alzheimer's disease compared to controls (Fig. 2C). Considering that we found accumulated insulin in Alzheimer's disease neurons, the increment in insulin levels quantified in brain extracts by ELISA could be underestimating the real levels of its accumulation in neurons.

Our ELISA results showing increased insulin levels in formic acid soluble fractions from Alzheimer's disease brains suggest accumulation of insulin in insoluble aggregates or fibrils in the disease. To further clarify this finding, we performed additional immunofluorescence experiments and analysed the samples by SIM microscopy. As shown in Fig. 2D, the pattern of insulin immunoreactivity in Alzheimer's disease samples does not correspond to mature fibrils. Moreover, insulin and phospho-tau (detected by AT180) immunoreactivities do not co-localize suggesting that insulin accumulation occurs independently of a physical interaction with phospho-tau oligomers or fibrils. To confirm the presence of insulin oligomers in human brain, we performed immunoprecipitation experiments with the anti-pan-oligomer conformational antibody A11. A11 has been used for detection of oligomeric structures, excluding monomers, protofibrils and fibrils (Upadhaya *et al.*, 2012). It has been shown to detect human insulin, IAPP, α-synuclein, polyglutamine, lysozyme and yeast prion oligomers (Kayed, 2003). Immunoprecipitation with A11 followed by blotting for insulin revealed the presence of insulin oligomers in human brain homogenates (Fig. 2E) (brain preparation corresponds to combined PBS and SDS fractions). Human recombinant insulin, either fresh or incubated (24 h, 37°C) for oligomerization, was used as a control. As seen in Fig. 2E (right blot), the IgG heavy chain was detected at ~50 kDa. In the sample with aggregated insulin, a signal was detected at 25 to 45 kDa, corresponding to insulin oligomers. Insulin oligomers were significantly higher in Alzheimer's disease compared to controls (Fig. 2E). To confirm these results, we performed immunoprecipitation with an insulin antibody followed by A11 blotting in non-denaturalizing conditions. As shown in Supplementary Fig. 1G, Alzheimer's disease samples showed increased levels of high molecular weight insulin oligomers (>100 kDa) compared to controls.

Neuronal accumulation of insulin in other tauopathies

Considering the strong relationship observed between insulin accumulation and tau hyperphosphorylation in Alzheimer's disease brains, we next analysed this

Figure 1 Continued

individual cells (>40 cells per patient) from CA1 of control and Alzheimer's disease patients (Braak I–II; Braak III–IV; Braak V–VI) show that insulin levels are increased along Alzheimer's disease progression. (**D**) Percentage of cells (>60 cells per patient) with basal versus increased insulin staining in CA1 of control and Alzheimer's disease patients with or without diabetes mellitus show that insulin accumulation is independent of the diabetic condition. (**E**) Confocal microscopy images of immunofluorescence staining against phospho-tau (AT180, red) and insulin (green) in hippocampal CA1 of control and Alzheimer's disease patients show intraneuronal insulin accumulation in AT180-positive neurons in Alzheimer's disease. DAPI was used as nuclear marker. Scale bar = 25 μm. (**F**) Percentage of cells that show hyperphosphorylated tau (AT180 positive), increased insulin levels or both in cingulate cortex, temporal cortex and hippocampal CA1 of controls and Alzheimer's disease. All data are represented as mean values ± SEM. ***$P < 0.001$ versus control, **$P < 0.01$ versus control, *$P < 0.05$ versus control. ABC = avidin-biotin complex; AD = Alzheimer's disease.

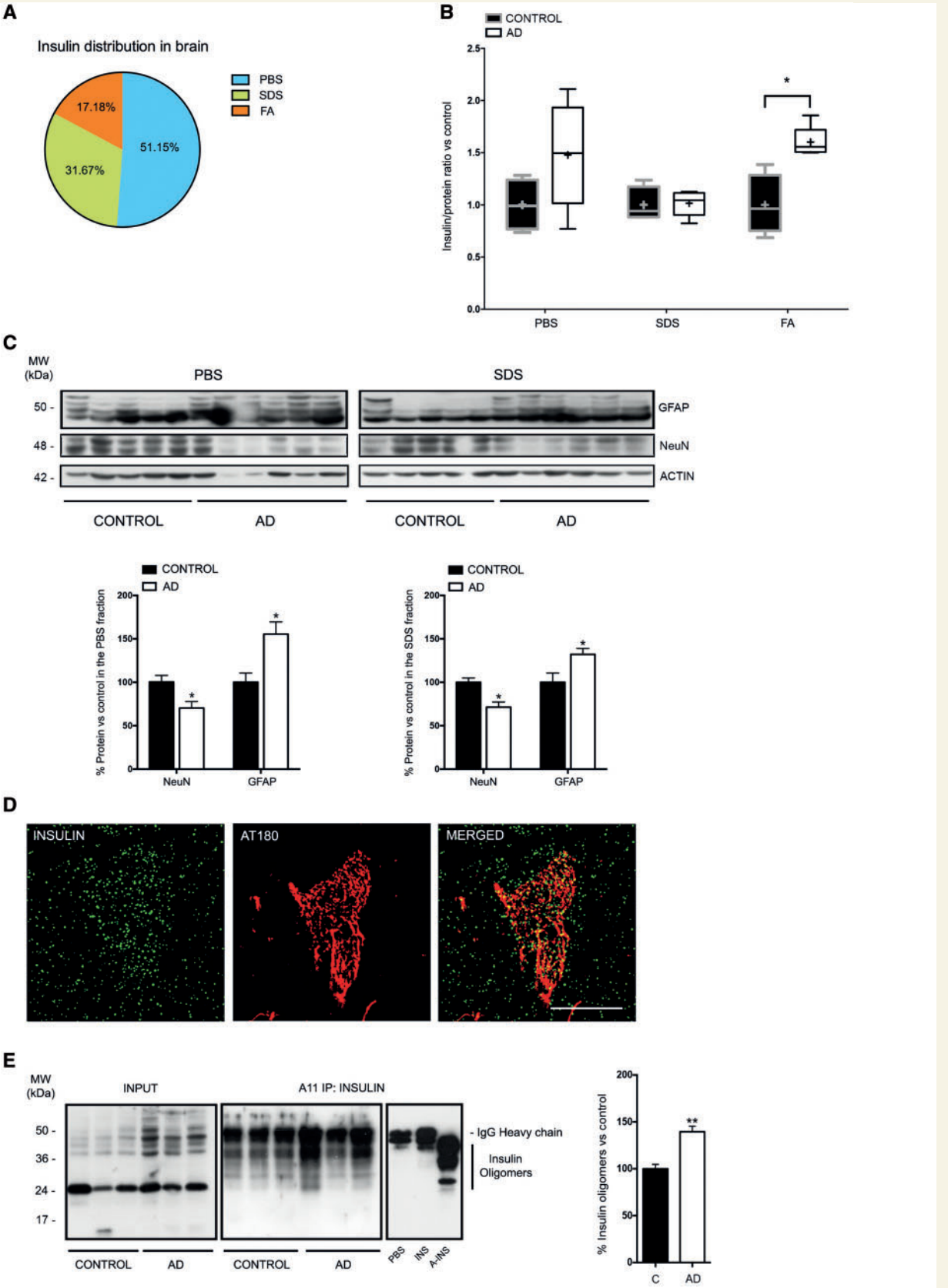

Figure 2 Insulin accumulates as insoluble oligomers in brain. (**A**) Insulin distribution in fractions (PBS, SDS and formic acid-soluble) of hippocampus from controls individuals. (**B**) Quantification of insulin in PBS, SDS and formic acid soluble fractions from hippocampus of controls (n = 6) and Alzheimer's disease (n = 5) patients shows increased insulin levels in the formic acid fraction in Alzheimer's disease compared to controls. Insulin levels were normalized per microgram of total protein in each fraction. (**C**) Immunoblotting for GFAP, NeuN and actin in the

(continued)

association in some of the most prevalent human tauopathies: AGD, PSP and corticobasal degeneration (CBD). AGD is a sporadic tauopathy characterized by the presence of argyrophilic grains in the neuropil (Ferrer *et al.*, 2008). PSP is a type of parkinsonism that, unlike Alzheimer's disease, presents additional tau deposits in glial cells both in the hippocampus and in neocortical and subcortical areas (Yoshida, 2006). Similar pathological features for tau accumulation are observed in CBD (Yoshida, 2006). As seen in Alzheimer's disease, all these tauopathies presented intraneuronal accumulation of insulin in NFT-bearing neurons in the CA1 layer of the hippocampus (Fig. 3A, B and Supplementary Fig. 2). In AGD, no increased insulin immunoreactivity was observed in argyrophilic grains or neuronal processes (Fig. 3A). These results are in agreement with our observations in Alzheimer's disease samples, where insulin staining was preferentially found in neuronal somas (Fig. 1E). Co-immunostainings with AT100 showed that all the cells labelled with AT180 also show AT100 immunoreactivity, discarding the possibility of identifying MAP2 as phospho-tau-positive cells (Supplementary Fig. 2A). As observed in Alzheimer's disease, CA1–CA3 hippocampal neurons with NFTs in AGD samples also showed increased Tau-1 immunoreactivity (Supplementary Fig. 2B). However, a different intracellular pattern between AT100 and AT180 was found in PSP and CBD (Supplementary Fig. 2A and B).

Indeed, the regulation of tau kinases and phosphatases by insulin is well known (Avila, 2008). To interrogate if tau hyperphosphorylation and insulin accumulation are separate events or cause and consequence of a common neurodegenerative mechanism, we compared brains of P301S mice—a model of tauopathy carrying a mutant (P301S) human *MAPT* gene encoding T34-tau isoform (1N4R) (Yoshiyama *et al.*, 2007) with brains of wild-type (C57) and Tau KO mice (Dawson *et al.*, 2001). In P301S mice, the development of tau pathology most likely occurs before any other neuropathological event due to the genetic background, and thus we could assess if tau hyperphosphorylation leads to insulin accumulation. AT180, AT100 and Tau-1 immunoreactivities were increased in CA1 hippocampal neurons together with insulin staining in P301S compared to C57 and Tau KO mice, where insulin levels where almost non-detectable (Fig. 3C and Supplementary Fig. 3), suggesting that phospho-tau accumulation precedes insulin accumulation in neurons.

Tau hyperphosphorylation results in intraneuronal accumulation of insulin oligomers and in insulin signalling deficits

We next established two cellular models of tau hyperphosphorylation; treatment of rat cortical neurons in primary culture with the phosphatase inhibitor okadaic acid (OA; 250 nM, 1h) (Pérez *et al.*, 2002; Broetto *et al.*, 2016) and overexpression of full-length tau in SH-SY5Y human neuroblastoma cells (Monroy-Ramírez *et al.*, 2013). As seen by immunoblotting, immunofluorescence and SIM microscopy, okadaic acid treatment resulted in accumulation of insulin, hyperphosphorylated tau and tau inside neurons (Fig. 4A and B). In agreement with results seen in Alzheimer's disease and human tauopathies (Figs 2D and 3A), intracellular insulin was not associated to tau fibrils (Fig. 4B). Immunoprecipitation with the A11 conformational antibody revealed the presence of insulin oligomers in primary neurons, which were increased upon okadaic acid treatment (Fig. 4C). To clarify whether insulin accumulation was directly dependent on tau hyperphosphorylation or just an additional consequence of phosphatase inhibition, we performed okadaic acid treatments under tau silencing conditions. As observed in Fig. 4D, silencing tau by ~50% prevented okadaic acid-induced insulin accumulation in neurons. Furthermore, overexpression of full-length tau in SH-SY5Y human neuroblastoma cells resulted in strong intracellular accumulations of hyperphosphorylated tau and insulin (Supplementary Fig. 4D). Okadaic acid-treated neurons and Tau-SH-SY5Y cells show both increased tau hyperphosphorylation and total tau accumulation. To clarify if intracellular insulin accumulation was mediated by tau hyperphosphorylation or its accumulation, we transfected SH-SY5Y cells with plasmids encoding GFP-tagged human tau (pRK5-EGFP-Tau), GFP-tagged pseudo-phosphorylated tau (pRK5-EGFP-Tau E14) and GFP-tagged phospho-null tau (pRK5-EGFP-Tau AP) (Hoover *et al.*, 2010). As shown in Supplementary Fig. 4I, insulin levels were significantly increased in pseudo-phosphorylated tau and total tau over-expressing SH-SY5Y cells. Supplementary Fig. 4J shows densitometric data of insulin normalized by tau levels in each of the three tau-overexpressing models. Both total tau and pseudo-phosphorylated tau significantly increased insulin levels when compared to phospho-null tau overexpressing SH-SY5Y cells.

Figure 2 Continued

same PBS and SDS fractions used for ELISA in **B**. (**D**) SIM super resolution image shows that insulin (green) is not forming mature fibrils or binding hyperphosphorylated tau (AT180, red) in Alzheimer's disease. Scale bar = 10 μm. (**E**) Immunoprecipitation of pooled PBS- and SDS- soluble hippocampal samples from Alzheimer's disease and control patients with the A11 anti-oligomer antibody followed by immunoblotting against insulin. Alzheimer's disease brains showed increased levels of insulin oligomers compared to controls (middle blot and histogram). PBS, human recombinant insulin (INS) and the same concentration of *in vitro* aggregated human recombinant insulin (A-INS) were used as positive (A-INS) and negative (PBS and INS) controls. Insulin oligomers are detected in bands between 20 and 50 kDa. An aliquot of each supernatant incubated for the immunoprecipitation followed by actin immunoblotting was used as loading control (INPUT). Data are represented as mean values ± SEM. $^{*}P < 0.05$ versus control, $^{**}P < 0.01$ versus control, $^{***}P < 0.001$ versus control; $n = 3$. AD = Alzheimer's disease; C = control; FA = formic acid.

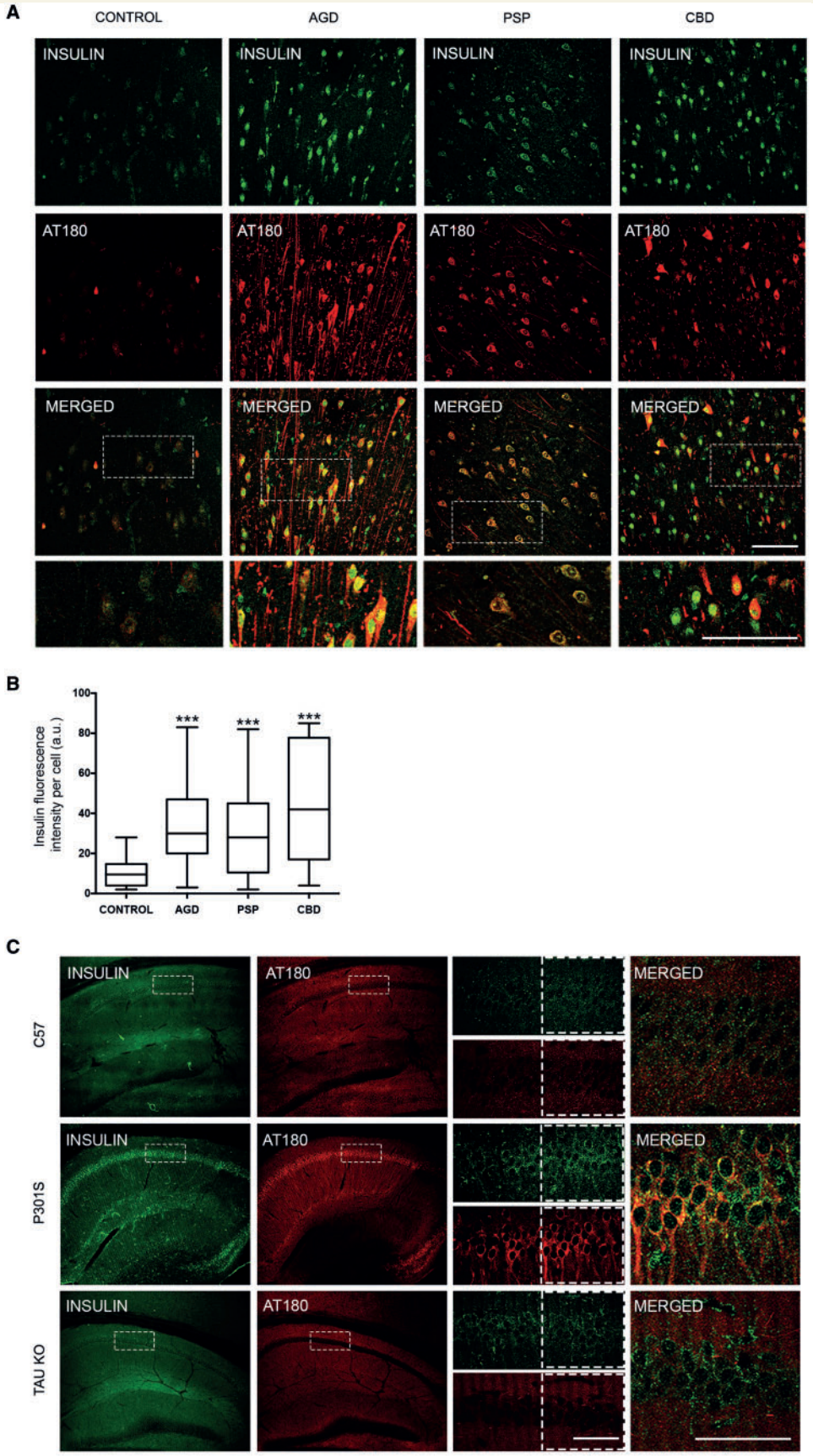

Figure 3 Insulin accumulates in human tauopathies and in P301S mice. (**A**) Confocal microscopy images of insulin (green), and hyperphosphorylated tau (AT180, red) in CA1 hippocampal brain sections of controls, and patients with AGD, PSP or CBD. Scale bar = 150 μm.

(continued)

As shown in Fig. 4E, no significant differences were found in IDE protein levels between control and okadaic acid treated neurons, suggesting that alterations in IDE expression, which could lead to deficiencies in insulin degradation, do not account for the results presented previously. Therefore, we next aimed to determine whether the origin of the high insulin levels observed in phospho-tau bearing neurons was enhanced insulin uptake or increased insulin synthesis. We used an antibody-free approach, incubating rat primary neurons with FITC-insulin (400 nM) either in the presence or absence of okadaic acid (250 nM, 1 h) and measured intracellular insulin fluorescence by flow cytometry. As shown in Fig. 4F, after only 1 h treatment with okadaic acid a modest but significant increase in FITC-insulin was found inside the cells. On the other hand, Q-PCR analysis revealed that okadaic acid treatment did not induce insulin synthesis, which was almost non-detectable (data not shown).

We finally aimed to clarify the consequences of insulin accumulation for insulin signalling in the cell. Western blot analysis revealed a dramatic decrease in insulin receptor expression and protein levels in tau-overexpressing SH-SY5Y cells (Supplementary Fig. 4E and G). Furthermore, these cells also show deficiencies downstream of the insulin receptor in the expression levels of GLUT4 (Supplementary Fig. 4F) and phosphorylation level of AKT (Supplementary Fig. 4H). In contrast, these effects on insulin receptor were not seen in primary neurons treated with okadaic acid (250 nM) for 1 h (Supplementary Fig. 4A and B). To clarify whether the decrease of insulin receptor levels was time-dependent, we treated neurons with a milder concentration of okadaic acid (10 nM) for a longer time (24 h). This condition resulted in accumulation of phosphorylated tau (Supplementary Fig. 4C), and a significant decrease in insulin receptor protein levels in neurons (Fig. 4G). To determine whether insulin receptor levels were downregulated as a consequence of the okadaic acid-mediated enhancement of insulin uptake, we incubated neurons for 24 h in insulin-free media, either in the presence or absence of okadaic acid. As shown in Fig. 4G, removing insulin from the media resulted in increased insulin receptor levels in control cells and prevented the okadaic acid-driven decrease in insulin receptor levels observed in the presence of insulin (Fig. 4H).

Discussion

Insulin signalling alterations and insulin resistance have been proposed as contributors to Alzheimer's disease pathogenesis, but the molecular mechanisms behind this association remain largely unknown. Here we report that insulin accumulates intraneuronally together with hyperphosphorylated tau in Alzheimer's disease and several tauopathies. In Alzheimer's disease, tau pathology initiates in the entorhinal cortex, followed by the hippocampus and reaching neocortical regions in the most advanced stages of the disease (Braak and Braak, 1996). These different stages of tau pathology correlate with the disease temporal course and serve to classify its progression from very early Alzheimer's disease (Braak I–II) to severe Alzheimer's disease (Braak V). We have found insulin accumulation in CA1-CA3 hippocampal neurons from very early stages of the disease (Braak I–II), to later disease stages in pyramid-like cortical neurons in the temporal neocortex. No significant insulin accumulation was found in the cingulate cortex, an area with late tau pathology in Alzheimer's disease. Accumulation of insulin observed in Alzheimer's disease brains occurs independently of whether the patient had diabetes mellitus or not, which is in agreement with previous reports showing that peripheral and brain insulin levels are independent, and brain insulin signalling alterations can occur independently of the presence of clinical diabetes (Talbot *et al.*, 2012).

Insulin levels have been shown to be decreased in the CSF of Alzheimer's disease individuals (Gil-Bea *et al.*, 2010; Lee *et al.*, 2013). These studies seem paradoxical with the results presented here and with previous evidence of increased general blood–brain barrier permeability in Alzheimer's disease (van de Haar *et al.*, 2016) and increased insulin blood–brain barrier permeability described in Alzheimer's disease mouse models (Poduslo *et al.*, 2001). A possibility to harmonize these seemingly conflicting results would be that the accumulation of insulin in Alzheimer's disease brains resulted from increased retention due to deficiencies in degradation or in clearance mechanisms. Indeed, this is the case with amyloid-β whose increased oligomeric and fibrillary forms in Alzheimer's disease brains are in contrast with its decreased levels in CSF (Gil-Bea *et al.*, 2010). Also, insulin is well known to undergo amyloid oligomerization and fibrillation *in vitro*, which leads to a loss of its activity (Hjorth *et al.*, 2016). While some authors have reported the presence of insulin aggregates in the injection area of diabetic patients (Mangla *et al.*, 2016), to date there are no reports showing endogenous insulin aggregation *in vivo*. Our SIM results suggest that insulin does not form mature fibrils in Alzheimer's disease brains. However, quantification of insulin levels by ELISA in different solubility fractions revealed that

Figure 3 Continued

(**B**) Insulin fluorescence intensity quantification from confocal images in individual cells (>40 cells per patient) from the CA1 layer of the hippocampus of control, AGD, PSP and CBD patients show that insulin levels are significantly increased in these taupathies. (**C**) Confocal microscopy images of brain slices from wild-type (C57), P301S and Tau KO mice stained with insulin (green) and hyperphosphorylated tau (AT180, red) show that insulin is accumulated in the hippocampus in P301S mice, together with tau. Scale bar = 60 μm.

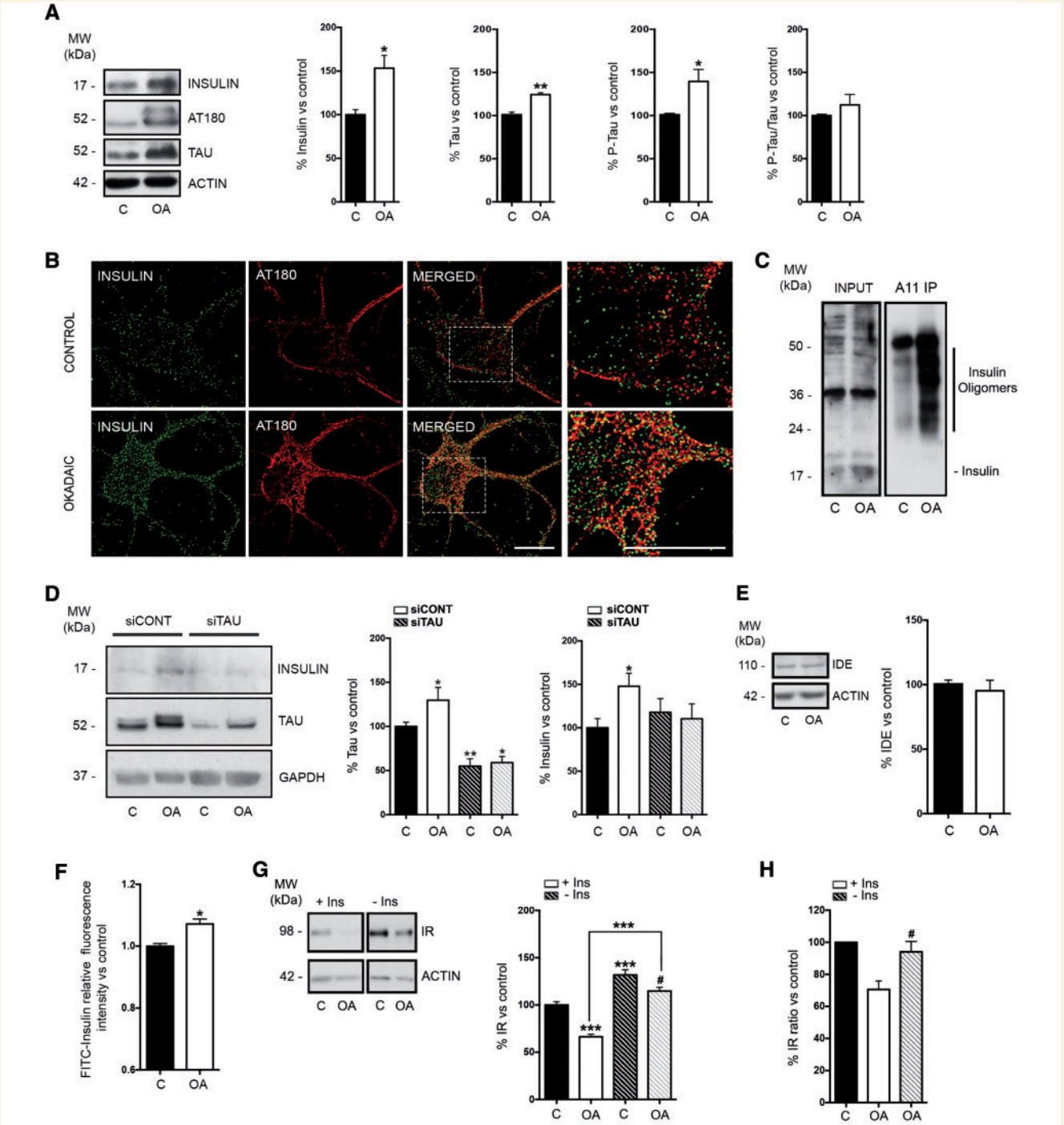

Figure 4 Tau hyperphosphorylation results in intraneuronal oligomerization of insulin and insulin resistance. (**A**) Immunoblotting against insulin, phospho-tau (AT180) and total tau (TAU) shows tau hyperphosphorylation and accumulation accompanied by increased insulin levels upon okadaic acid treatment (OA, 250 nM, 1 h) in primary rat cortical neurons. (**B**) SIM images of immunofluorescence against insulin (green) and phospho-tau (AT180, red) in controls and in primary neurons treated with okadaic acid (OA, 250 nM, 1 h). Scale bar = 10 μm. (**C**) Immunoprecipitation with the A11 anti-oligomer antibody followed by SDS gel electrophoresis and insulin immunoblotting (*right* blot) shows that insulin is generating oligomers upon okadaic acid treatment in cortical neurons in primary culture. Input samples blotted for insulin are shown in the *left* blot. (**D**) Immunoblotting from cortical neuron lysates shows that siRNA silencing of Tau prevents the effect of okadaic acid on insulin accumulation. Histograms show quantifications of Tau and insulin with data as percentage of control values. (**E**) Immunoblotting against IDE shows no differences in protein levels in okadaic acid (250 nM, 1 h) treated cortical neurons compared to controls. Actin is shown as loading control. (**F**) Flow cytometry assessment of FITC-insulin fluorescence intensity show that okadaic acid (250 nM, 1 h) induces an increase in FITC-insulin levels in cortical primary neurons. (**G**) Immunoblotting against insulin receptor shows a significant decrease in protein levels in okadaic acid (10 nM, 24 h) treated cortical neurons compared to controls. This effect is partially prevented in insulin-free (−Ins) conditions. (**H**) Data from **G** expressed as ratio of insulin receptor protein levels in okadaic acid-treated versus respective controls in each experiment, either in the presence

(continued)

insulin is accumulating in the insoluble fraction (formic acid soluble) in Alzheimer's disease brains. Moreover, immunoprecipitation with the anti-pan-oligomer conformational antibody A11 showed the presence of brain insulin oligomers, with increased concentrations in Alzheimer's disease samples. Immunoprecipitation with insulin followed by A11 blotting under non-denaturalizing conditions confirmed the presence of increased levels of insulin oligomers in Alzheimer's disease samples. It has been previously shown that SDS destroys amyloid-β native high molecular weight aggregates (Yoshiike *et al.*, 2008; Upadhaya *et al.*, 2012). This might explain the different molecular weight for insulin oligomers observed under denaturalizing conditions (Fig. 2E) and native PAGE (Supplementary Fig. 1G). As seen for amyloid-β pathology, increased aggregation and retention in Alzheimer's disease could explain the decrease in CSF insulin levels despite increased blood–brain barrier permeability in the disease.

A previous report has shown signs of alterations in IRS1 serine phosphorylation, which is a marker for insulin resistance, in different tauopathies, including Alzheimer's disease, CBD and PSP (Yarchoan *et al.*, 2014). This effect was neuron-specific and was not found in other neurodegenerative disorders with no tau pathology, such as alpha synucleopathies or TDP-43 proteinopathies (Yarchoan *et al.*, 2014). We found insulin accumulation together with hyperphosphorylated tau in CA1–CA3 hippocampal neurons in CBD, PSP and AGD, which further suggests the existence of a very close relationship between both pathological outcomes. To further study this possibility, we used P301S mice (Yoshiyama *et al.*, 2007) and we found insulin accumulation in the hippocampus occurring in parallel to tau pathology. Similarly, accumulation of insulin was found in stable tau-overexpressing SH-SY5Y cells. Furthermore, in a cellular model of tau hyperphosphorylation, where rat cortical neurons were treated with the phosphatases inhibitor okadaic acid, we found that tau hyperphosphorylation was accompanied by insulin accumulation in the neurons. However, if okadaic acid was used under tau silencing conditions, the accumulation of insulin was not found, suggesting that tau pathology triggers insulin accumulation and oligomerization. In agreement with the results observed in Alzheimer's disease brains, okadaic acid treatment led to the development of intracellular tau fibres and insulin aggregates in neurons, identified as oligomeric by immunoprecipitation with the anti-pan-oligomers antibody A11. As seen in Alzheimer's disease brains, tau fibres and insulin oligomers did not co-localize in our cellular models. Using alternative *in vitro* models, we found that overexpression of total tau, or pseudo-phosphorylated tau resulted in a significant increase of intracellular insulin compared to both wild-type and overexpressing phospho-null tau cells. Together, our results suggest that tau hyperphosphorylation, rather that tau enhancement, drives insulin accumulation inside the cells.

IDE is the main enzyme responsible for insulin degradation (Farris *et al.*, 2003), and has been found to be decreased in the hippocampus of APOE4 carriers compared to non-APOE4 carriers in Alzheimer's disease (Cook *et al.*, 2003). However, others showed that IDE levels are unchanged in Alzheimer's disease brains compared to controls (Miners *et al.*, 2009). We found that okadaic acid treatment does not change IDE protein levels in primary neurons, suggesting that okadaic acid-induced intraneuronal insulin accumulation was not due to deficiencies in its degradation. As neurons in primary culture and hippocampal neurons in the brain have been reported to synthesize insulin (Steen *et al.*, 2005; Molnár *et al.*, 2014), we next interrogated if insulin accumulation was caused by increased insulin uptake or by increased synthesis. Incubation with FITC labelled human recombinant insulin in okadaic acid-treated neurons for 1 h revealed increased insulin uptake in these cells. Quantitative PCR analysis of insulin expression levels showed no differences in insulin synthesis, suggesting that the increased insulin levels observed in okadaic acid-treated neurons result from accumulation of extracellular insulin.

It is well known that insulin signalling alterations contribute to hyperphosphorylation and accumulation of tau (Avila, 2008; Liu *et al.*, 2009); on the other hand, the effect of tau alterations on insulin signalling is not sufficiently understood. We show that both tau-overexpressing SH-SY5Y cells and okadaic acid-treated neurons have decreased insulin receptor levels. Tau-overexpressing SH-SY5Y cells also showed a significant decrease in AKT phosphorylation and GLUT4 expression levels, which additionally support the concept that these cells have basal deficiencies in insulin signalling. Moreover, in okadaic acid-treated neurons, removing insulin from the media prevented the decrease in insulin receptor levels. This evidence suggests that cells suffering from tau hyperphosphorylation show enhanced insulin uptake, which in the long-term leads to insulin resistance.

In summary, our results demonstrate that tau hyperphosphorylation leads to increased uptake and accumulation of insulin as insoluble oligomeric aggregates inside neurons. Cells with accumulated insulin show decreased insulin receptor levels and signs of insulin resistance. Previous reports demonstrated the existence of insulin receptor downregulation, neuronal resistance to insulin and glucose hypometabolism in Alzheimer's disease and other tauopathies (Steen *et al.*, 2005; Molnár *et al.*, 2014), but the mechanisms

Figure 4 Continued
or absence (−Ins) of insulin in the media. Bars show mean values ± SEM of three independent experiments. $^{**}P < 0.01$ versus control, $^{*}P < 0.05$ versus control, $^{\#}P < 0.05$ versus its control (−Ins control).

remain to be fully understood. Our present study provides novel evidence suggesting accumulation of intraneuronal oligomeric insulin as a contributing factor to the insulin resistance reported in these diseases. Likewise, insulin accumulation could have functional consequences for insulin recycling, homeostasis and glucose metabolism in brain and contribute to these neurodegenerative processes. The results presented also suggest that the therapeutic use of insulin for the treatment of neurodegenerative disorders with associated tauopathy should be used with caution.

Acknowledgements

We would like to acknowledge Hans Blom, from the Superresolution Microscopy Science for Life Laboratory for his assistance and advice with the superresolution images and the Harvard Brain Tissue Resource Center for providing brain samples for protein determinations. We acknowledge Tomas Hökfelt for the supply of insulin antibody Ab909. This study was performed at the Live Cell Imaging facility, Karolinska Institutet, Sweden, supported by grants from the Knut and Alice Wallenberg Foundation, the Swedish Research Council, the Centre for Innovative Medicine and the Jonasson center at the Royal Institute of Technology, Sweden.

Funding

The Harvard Brain Tissue Resource Center is supported in part by PHS grant number R24MHO68855 for providing brain samples for protein determinations. P.M.S. was the recipient of the EMBO long-term fellowship (ALFT 696-2013) and the SSMF postdoctoral fellowship. This research was supported by the following Swedish foundations: Swedish Brain Power, the regional agreement on medical training and clinical research (ALF) between Stockholm County Council and Karolinska Institutet, Margaretha af Ugglas Foundation, Olle Engkvist Byggmästare Stiftelse, Gun och Bertil Stohnes Stiftelse, Loo och Hans Osterman Foundation, Karolinska Institutet fund for geriatric research, Stiftelsen Gamla Tjänarinnor, Riskbankens Jubileumfonden, Hjärnfonden and Alzheimerfonden.

Supplementary material

Supplementary material is available at *Brain* online.

References

Applied Biosystems. Guide to performing relative quantitation of gene expression using real-time quantitative PCR. Foster City: Applied Biosystems; 2004.

Avila J. Tau kinases and phosphatases. J Cell Mol Med 2008; 12: 258–9.

Bian H, Bian W, Lin X, Ma Z, Chen W, Pu Y. RNA Interference silencing of glycogen synthase kinase 3beta inhibites tau phosphorylation in mice with Alzheimer disease. Neurochem Res 2016; 41: 2470–80.

Braak H, Braak E. Evolution of the neuropathology of Alzheimer's disease. Acta Neurol Scand Suppl 1996; 165: 3–12.

Broetto N, Hansen F, Brolese G, Batassini C, Lirio F, Galland F, et al. Intracerebroventricular administration of okadaic acid induces hippocampal glucose uptake dysfunction and tau phosphorylation. Brain Res Bull 2016; 124: 136–43.

Calvo-Ochoa E, Hernández-Ortega K, Ferrera P, Morimoto S, Arias C. Short-term high-fat-and-fructose feeding produces insulin signaling alterations accompanied by neurite and synaptic reduction and astroglial activation in the rat hippocampus. J Cereb Blood Flow Metab 2014; 34: 1001–8.

Chiu SL, Chen CM, Cline HT. Insulin receptor signaling regulates synapse number, dendritic plasticity, and circuit function *in vivo*. Neuron 2008; 58: 708–19.

Cook DG, Leverenz JB, McMillan PJ, Kulstad JJ, Ericksen S, Roth RA, et al. Reduced hippocampal insulin-degrading enzyme in late-onset Alzheimer's disease is associated with the apolipoprotein E-epsilon4 allele. Am J Pathol 2003; 162: 313–19.

Dawson HN, Ferreira A, Eyster MV, Ghoshal N, Binder LI, Vitek MP. Inhibition of neuronal maturation in primary hippocampal neurons from tau deficient mice. J Cell Sci 2001; 114: 1179–87.

de la Monte SM, Re E, Longato L, Tong M. Dysfunctional pro-ceramide, ER stress, and insulin/IGF signaling networks with progression of Alzheimer's disease. J Alzheimers Dis 2012; 30: S217–29

de la Monte SM, Wands JR. Alzheimer's disease is type 3 diabetes-evidence reviewed. J Diabetes Sci Technol 2008; 2: 1101–13.

Devaskar SU, Giddings SJ, Rajakumar PA, Carnaghi LR, Menon RK, Zahm DS. Insulin gene expression and insulin synthesis in mammalian neuronal cells. J Biol Chem 1994; 269: 8445–54.

Farris W, Mansourian S, Chang Y, Lindsley L, Eckman EA, Frosch MP, et al. Insulin-degrading enzyme regulates the levels of insulin, amyloid beta-protein, and the beta-amyloid precursor protein intracellular domain *in vivo*. Proc Natl Acad Sci USA 2003; 100: 4162–7.

Ferrer I, Santpere G, Van Leeuwen FW. Argyrophilic grain disease. Brain 2008; 131: 1416–32.

García-Cáceres C, Quarta C, Varela L, Gao Y, Gruber T, Legutko B, et al. Astrocytic insulin signaling couples brain glucose uptake with nutrient availability. Cell 2016; 166: 867–80.

Gil-Bea FJ, Solas M, Solomon A, Mugueta C, Winblad B, Kivipelto M, et al. Insulin levels are decreased in the cerebrospinal fluid of women with prodomal Alzheimer's disease. J Alzheimers Dis 2010; 22: 405–13.

Gustafsson MG. Surpassing the lateral resolution limit by a factor of two using structured illumination microscopy. J Microsc 2000; 198: 82–7.

Hjorth CF, Norrman M, Wahlund PO, Benie AJ, Petersen BO, Jessen CM, et al. Structure, Aggregation, and activity of a covalent insulin dimer formed during storage of neutral formulation of human insulin. J Pharm Sci 2016; 105: 1376–86.

Hoover BR, Reed MN, Su J, Penrod RD, Kotilinek LA, Grant MK, et al. Tau mislocalization to dendritic spines mediates synaptic dysfunction independently of neurodegeneration. Neuron 2010; 68: 1067–81.

Kapogiannis D, Boxer A, Schwartz JB, Abner EL, Biragyn A, Masharani U, et al. Dysfunctionally phosphorylated type 1 insulin receptor substrate in neural-derived blood exosomes of preclinical Alzheimer's disease. FASEB J 2015; 29: 589–96.

Kayed R, Head E, Thompson JL, McIntire TM, Milton SC, Cotman CW, et al. Common structure of soluble amyloid oligomers implies common mechanism of pathogenesis. Science 2003; 300: 486–9.

Kennedy L, Pham SC, Grishok A. Nonautonomous regulation of neuronal migration by insulin signaling, DAF-16/FOXO, and PAK-1. Cell Rep 2013; 4: 996–1009.

Kim B, Figueroa-Romero C, Pacut C, Backus C, Feldman EL. Insulin resistance prevents AMPK-induced tau dephosphorylation through akt-mediated increase in AMPK$^{Ser\text{-}485}$ phosphorylation. J Biol Chem 2015; 290: 19146–57.

Komis G, Šamajová O, Ovečka M, Šamaj J. Super-resolution microscopy in plant cell imaging. Trends Plant Sci 2015; 20: 834–43.

Lee S, Tong M, Hang S, Deochand C, de la Monte S. CSF and brain indices of insulin resistance, oxidative stress and neuro-inflammation in early versus late Alzheimer's disease. J Alzheimers Dis Park 2013; 3: 128.

Lin JW, Ju W, Foster K, Lee SH, Ahmadian G, Wyszynski M, et al. Distinct molecular mechanisms and divergent endocytotic pathways of AMPA receptor internalization. Nat Neurosci 2000; 3: 1282–90.

Liu F, Iqbal K, Grundke-Iqbal I, Hart GW, Gong CX. O-GlcNAcylation regulates phosphorylation of tau: a mechanism involved in Alzheimer's disease. Proc Natl Acad Sci USA 2004; 101: 10804–9.

Liu F, Shi J, Tanimukai H, Gu J, Gu J, Grundke-Iqbal I, et al. Reduced O-GlcNAcylation links lower brain glucose metabolism and tau pathology in Alzheimer's disease. Brain 2009; 132: 1820–32.

Liu R, Zhou XW, Tanila H, Bjorkdahl C, Wang JZ, Guan ZZ, et al. Phosphorylated PP2A (tyrosine 307) is associated with Alzheimer neurofibrillary pathology. In Focus. J Cell Mol Med 2008; 12: 241–57.

Luchsinger JA, Tang MX, Shea S, Mayeux R. Hyperinsulinemia and risk of Alzheimer disease. Neurology 2004; 63: 1187–92.

Mangla A, Kim GJ, Agarwal N, Khurana S, Catchatourian R, Jiang JJ. Localized insulin amyloidosis with use of concentrated insulin: a potential complication. Diabet Med 2016; 33: e32–5.

Miners JS, Baig S, Tayler H, Kehoe PG, Love S. Neprilysin and insulin-degrading enzyme levels are increased in Alzheimer disease in relation to disease severity. J Neuropathol Exp Neurol 2009; 68: 902–14.

Molnár G, Faragó N, Kocsis ÁK, Rózsa M, Lovas S, Boldog E, et al. GABAergic neurogliaform cells represent local sources of insulin in the cerebral cortex. J Neurosci 2014; 34: 1133–7.

Monroy-Ramírez HC, Basurto-Islas G, Mena R, Cisneros B, Binder LI, Avila J, et al. Alterations in the nuclear architecture produced by the overexpression of tau protein in neuroblastoma cells. J Alzheimers Dis 2013; 36: 503–20.

Mullins RJ, Mustapic M, Goetz EJ, Kapogiannis D. Exosomal biomarkers of brain insulin resistance associated with regional atrophy in Alzheimer's disease. Hum Brain Mapp 2017; 38: 1933–40.

Pandini G, Pace V, Copani A, Squatrito S, Milardi D, Vigneri R. Insulin has multiple antiamyloidogenic effects on human neuronal cells. Endocrinology 2013; 154: 375–87.

Pérez M, Hernández F, Gómez-Ramos A, Smith M, Perry G, Avila J. Formation of aberrant phosphotau fibrillar polymers in neural cultured cells. Eur J Biochem 2002; 269: 1484–9.

Poduslo JF, Curran GL, Wengenack TM, Malester B, Duff K. Permeability of proteins at the blood-brain barrier in the normal adult mouse and double transgenic mouse model of Alzheimer's disease. Neurobiol Dis 2001; 8: 555–67.

Rivera EJ, Goldin A, Fulmer N, Tavares R, Wands JR, de la Monte SM. Insulin and insulin-like growth factor expression and function deteriorate with progression of Alzheimer's disease: link to brain reductions in acetylcholine. J Alzheimers Dis 2005; 8: 247–68.

Sandebring A, Welander H, Winblad B, Graff C, Tjernberg LO. The pathogenic abeta43 is enriched in familial and sporadic Alzheimer disease. PLoS One 2013; 8: e55847.

Schermelleh L, Heintzmann R, Leonhardt H. A guide to super-resolution fluorescence microscopy. J Cell Biol 2010; 190: 165–75.

Schubert M, Gautam D, Surjo D, Ueki K, Baudler S, Schubert D, et al. Role for neuronal insulin resistance in neurodegenerative diseases. Proc Natl Acad Sci USA 2004; 101: 3100–5.

Skeberdis VA, Lan J, Zheng X, Zukin RS, Bennett MV. Insulin promotes rapid delivery of N-methyl-D- aspartate receptors to the cell surface by exocytosis. Proc Natl Acad Sci USA 2001; 98: 3561–6.

Steen E, Terry BM, Rivera EJ, Cannon JL, Neely TR, Tavares R, et al. Impaired insulin and insulin-like growth factor expression and signaling mechanisms in Alzheimer's disease–is this type 3 diabetes? J Alzheimers Dis 2005; 7: 63–80.

Talbot K, Wang HY, Kazi H, Han LY, Bakshi KP, Stucky A, et al. Demonstrated brain insulin resistance in Alzheimer's disease patients is associated with IGF-1 resistance, IRS-1 dysregulation, and cognitive decline. J Clin Invest 2012; 122: 1316–38.

Upadhaya AR, Lungrin I, Yamaguchi H, Fändrich M, Thal DR. High-molecular weight Aβ oligomers and protofibrils are the predominant Aβ species in the native soluble protein fraction of the AD brain. J Cell Mol Med 2012; 16: 287–95.

van de Haar HJ, Burgmans S, Jansen JF, van Osch MJ, van Buchem MA, Muller M, et al. Blood-brain barrier leakage in patients with early Alzheimer disease. Radiology 2016; 281: 527–35.

Wegel E, Göhler A, Lagerholm BC, Wainman A, Uphoff S, Kaufmann R, et al. Imaging cellular structures in super-resolution with SIM, STED and localisation microscopy: a practical comparison. Sci Rep 2016; 6: 27290.

Willette AA, Bendlin BB, Starks EJ, Birdsill AC, Johnson SC, Christian BT, et al. Association of insulin resistance with cerebral glucose uptake in late middle–aged adults at risk for Alzheimer disease. JAMA Neurol 2015a; 72: 1013.

Willette AA, Johnson SC, Birdsill AC, Sager MA, Christian B, Baker LD, et al. Insulin resistance predicts brain amyloid deposition in late middle-aged adults. Alzheimers Dement 2015b; 11: 504–10.

Williamson DF, Parker RA, Kendrick JS. The box plot: a simple visual method to interpret data. Ann Intern Med 1989; 110: 916–21.

Xie C, Miyasaka T. The role of the carboxyl-terminal sequence of tau and MAP2 in the pathogenesis of dementia. Front Mol Neurosci 2016; 9: 158.

Xu WL, Qiu CX, Wahlin A, Winblad B, Fratiglioni L. Diabetes mellitus and risk of dementia in the Kungsholmen project: a 6-year follow-up study. Neurology 2004; 63: 1181–6.

Yarchoan M, Toledo JB, Lee EB, Arvanitakis Z, Kazi H, Han LY, et al. Abnormal serine phosphorylation of insulin receptor substrate 1 is associated with tau pathology in Alzheimer's disease and tauopathies. Acta Neuropathol 2014; 128: 679–89.

Yoshida M. Cellular tau pathology and immunohistochemical study of tau isoforms in sporadic tauopathies. Neuropathology 2006; 26: 457–70.

Yoshiike Y, Minai R, Matsuo Y, Chen YR, Kimura T, Takashima A. Amyloid oligomer conformation in a group of natively folded proteins. PLoS One 2008; 3: e3235.

Yoshiyama Y, Higuchi M, Zhang B, Huang SM, Iwata N, Saido TC, et al. Synapse loss and microglial activation precede tangles in a P301S tauopathy mouse model. Neuron 2007; 53: 337–51.

Yuzwa SA, Vocadlo DJ. O-GlcNAc and neurodegeneration: biochemical mechanisms and potential roles in Alzheimer's disease and beyond. Chem Soc Rev 2014; 43: 6839–58.

Zhao L, Teter B, Morihara T, Lim GP, Ambegaokar SS, Ubeda OJ, et al. Insulin-degrading enzyme as a downstream target of insulin receptor signaling cascade: implications for Alzheimer's disease intervention. J Neurosci 2004; 24: 11120–6.

Zhao W, Wu X, Xie H, Ke Y, Yung WH. Permissive role of insulin in the expression of long-term potentiation in the hippocampus of immature rats. Neurosignals 2011; 18: 236–45.

Zhao WQ, Lacor PN, Chen H, Lambert MP, Quon MJ, Krafft GA, et al. Insulin receptor dysfunction impairs cellular clearance of neurotoxic oligomeric Aβ. J Biol Chem 2009; 284: 18742–53.